IJMMM International Journal of Minerals, Metallurgy and Materials 矿物冶金与材料学报（英文版）

High toughness and strong electromagnetic shielding properties of PAM/PEG dual network hydrogels

Kunlan Diao, Yuhuan Xu, Jingyu Du, Teng Zhou, Xiao Zhan, Daohai Zhang, Xiaosi Qi, and Shuhao Qin

Cite this article as:
Kunlan Diao, Yuhuan Xu, Jingyu Du, Teng Zhou, Xiao Zhan, Daohai Zhang, Xiaosi Qi, and Shuhao Qin, High toughness and strong electromagnetic shielding properties of PAM/PEG dual network hydrogels, *Int. J. Miner. Metall. Mater.*, 32(2025), No. 3, pp. 747-755. https://doi.org/10.1007/s12613-024-3012-7

View the article online at SpringerLink or IJMMM Webpage.

INTERNATIONAL JOURNAL OF
Minerals, Metallurgy and Materials

Volume 32, Number 3, March 2025
Page 747

Research Article https://doi.org/10.1007/s12613-024-3012-7

High toughness and strong electromagnetic shielding properties of PAM/PEG dual network hydrogels

Kunlan Diao[1)], *Yuhuan Xu*[1)], *Jingyu Du*[1)], *Teng Zhou*[1)], *Xiao Zhan*[1)], *Daohai Zhang*[1),✉], *Xiaosi Qi*[2),✉], *and Shuhao Qin*[3),✉]

1) School of Chemical Engineering, Guizhou Minzu University, Guiyang 550025, China
2) College of Physics, Guizhou University, Guiyang 550025, China
3) National Engineering Research Center for Compounding and Modification of Polymer Materials, Guiyang 550014, China
(Received: 12 June 2024; revised: 12 September 2024; accepted: 18 September 2024)

Abstract: With the wide application of electromagnetic wave, a high performance electromagnetic shielding material is urgently needed to solve the harm caused by electromagnetic wave. Complete cross-linking strategy is adopted in this paper. Polyacrylamide (PAM) was synthesized by *in-situ* polymerization of acrylamide (AM) monomer. The obtained PAM was blended with polyethylene glycol (PEG) to prepare PAM/PEG hydrogels and form rigid support structures. Subsequently, the modified carbon nanotubes (S-CNTs) were incorporated into sodium alginate (SA) and PAM/PEG. Finally, Na^+ was used to trigger SA self-assembly, which significantly improved the mechanical properties and electrical conductivity of the hydrogels, and prepared PAM/PEG/SA/S-CNTs-Na hydrogels with high toughness and strong electromagnetic interference (EMI) shielding efficiency (SE). The results showed that the compressive strength of PAM/PEG/SA/S-CNTs-Na hydrogel was 19.05 MPa, which was 7.69% higher than that of PAM/PEG hydrogel (17.69 MPa). More encouraging, the average EMI SE of PAM/PEG/SA/S-CNTs-Na hydrogels at a thickness of only 3 mm and a CNTs content of 16.53wt% was 32.92 dB, which is 113.21% higher than that of PAM/PEG hydrogels (15.44 dB).

Keywords: polyacrylamide; polyethylene glycol; sodium alginate; carbon nanotubes; electromagnetic shielding

1. Introduction

With the wide use of communication technology such as computer and mobile phone, people's daily life and electromagnetic wave have been inseparable. Electromagnetic wave can quickly transmit information and energy, so it is widely used in electronic and electrical engineering, radio communication, medicine, military, and other fields [1–5]. However, electromagnetic wave brings convenience to our life but also brings a lot of harm. For example, the interweaving of different electromagnetic (EM) signals can cause signal distortion [6–7]. If the body absorbs harmful electromagnetic radiation, it will lead to cancer, mental disorders, fetal abnormalities, cardiovascular diseases, and other diseases [8–9]. Various EM radiation sources will cause environmental pollution. Therefore, the harm caused by electromagnetic radiation must be solved immediately, and the use of electromagnetic protective materials (including electromagnetic shielding materials and absorbing materials) to "cut off" the transmission path of electromagnetic waves can effectively protect sensitive objects from the impact of electromagnetic radiation, which is the main way to solve electromagnetic hazards.

Traditional metal materials (such as silver, copper, iron, nickel, and their alloys) are usually used as equipment shielding shells. However, metal-based materials have disadvantages such as poor thermal stability, high density, and high mechanical stress, which limit their application in electromagnetic shielding field [10–13]. Therefore, it is urgent to develop an advanced electromagnetic shielding material with easy machining, high mechanical flexibility, and high controllable electromagnetic shielding efficiency. Studies have found that hydrogel materials have arbitrary shape adaptability and self-healing ability [14–15]. Their internal contains rich water groups, can absorb electromagnetic waves, in addition, hydrogels are easy to fill other functional fillers for modification. Therefore, hydrogel materials have great application prospects in wearable electronic products, aerospace fields, and electromagnetic shielding fields. Polyacrylamide (PAM) is a kind of hydrophilic polymer that has been widely studied. Its internal crosslinking network contains reactive groups such as amide bonds, which is conducive to the formation of hydrogen bonds and the chemical modifications with various types [16–17]. However, PAM hydrogel itself lacks conductive and sufficient electromagnetic shielding properties. Therefore, it is necessary to incorporate relevant functional fillers to impart conductive and

✉ Corresponding authors: Daohai Zhang E-mail: zhangdaohai6235@163.com; Xiaosi Qi E-mail: xsqi@gzu.edu.cn; Shuhao Qin E-mail: qinshuhao@126.com

electromagnetic shielding ability. Yang *et al.* [18] incorporated multi-walled carbon nanotubes (MWCNT) into hydrophobic association PAM hydrogels, and cellulose nanofibers (CNF) were used as dispersants. The optimal tensile strength and conductivity of PAM/CNF/MWCNT composite hydrogels were 0.24 MPa and 0.85 s/m, respectively. The electromagnetic interference (EMI) shielding efficiency (SE) is 28.5 dB. On this basis, Lu *et al.* [19] used a simple strategy to prepare polypyrrole nanotube–polyethylene glycol–polyvinyl alcohol hydrogel (PPPg). When the prepared hydrogel was in the X-band and the thickness was 2 mm, the EMI SE could reach 21 dB. In addition, this film has excellent flexibility, with an elastic deformation of 100.9% at 2.28 MPa. In addition, Zhou *et al.* [20] prepared Fe_3O_4@RGO/PAM conductive hydrogel by using the hydrothermal synthesis method Fe_3O_4@RGO as the precursor. The conductivity of the hydrogel reaches 16.2 s/m at 3 mm thickness, and the maximum EMI SE is 27.1 dB. It has been found that although carbon nanotubes (CNTs) have been widely used because of their mechanical and electrical properties such as high specific structure, durability, and high electrical conductivity. Unfortunately, the accumulation of hydrophobic carbon nanotubes weakens the mechanical and electrical properties of hydrogels [21–22]. It is worth mentioning that the abundant oxygen functional groups (=O, −OH, and −COO−) in sodium alginate (SA) easily form hydrogen bond interactions with termination groups on the surface of CNTs, thus improving the interface mechanical properties between CNTs and SA [23–24]. In addition, it can bind to metal cations and induce SA self-assembly, resulting in greater internal density, which is conducive to the free movement of electrons. Therefore, it is often used as a biological material with a promising function or other materials doping.

In this paper, PAM/PEG/SA/S-CNTs-Na hydrogels with high toughness and strong EMI SE were prepared by a clever strategy of complete cross-linking. Firstly, acrylamide (AM) monomer was thermally induced free radical *in situ* polymerization to produce PAM, which was then mixed with polyethylene glycol (PEG) to form rigid PAM/PEG support structure. Secondly, the dispersion of CNTs was promoted after the functionalization of SA and hydroxyl (–OH) groups by non-covalent grafting. Then, anionic surfactant sodium dodecyl benzene sulfonate (SDBS) was used as modifier to inhibit the agglomeration of CNTs. Finally, the mechanical properties, conductance, and electromagnetic shielding properties of the hydrogel were significantly improved by SA self-assembly induced by Na^+ immersion method.

2. Experimental

As shown in Fig. 1, hydrogels of PAM/PEG, PAM/PEG/SA, PAM/PEG/SA/CNTs, and PAM/PEG/SA/S-CNTs were prepared by thermal initiated *in-situ* polymerization. Taking PAM/PEG/SA/S-CNTs hydrogel as an example, AM, SA, and PEG were first dissolved in deionized water to form a homogeneous solution, and then SDBS modified CNTs were added. After magnetic stirring for 1 h, CNTs were poured into a silica gel. PAM/PEG/SA/S-CNTs hydrogel was obtained after thermal polymerization at 70°C for 5 h. Then PAM/PEG/SA, PAM/PEG/SA/CNTs, and PAM/PEG/SA/S-

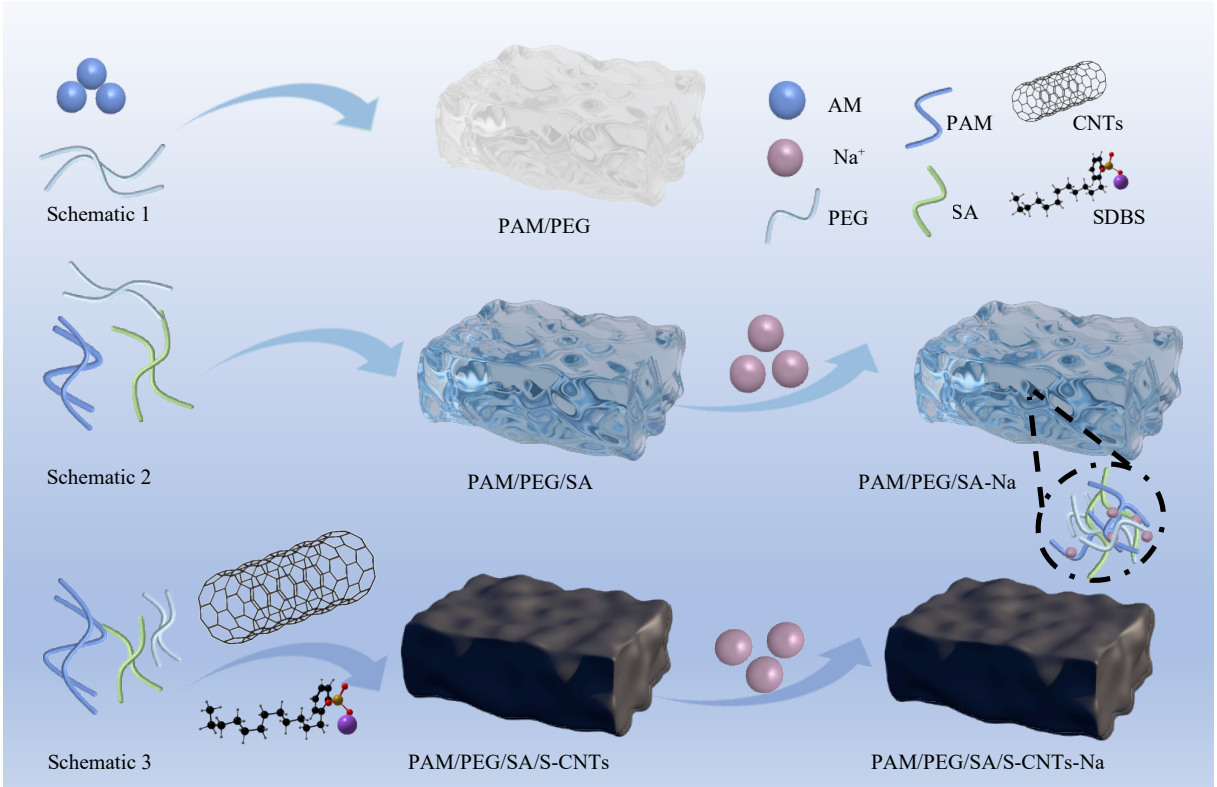

Fig. 1. Schematics of technical route for preparing PAM/PEG, PAM/PEG/SA, PAM/PEG/SA-Na, PAM/PEG/SA/S-CNTs, and PAM/PEG/SA/S-CNTs-Na hydrogels.

CNTs hydrogels were immersed in saturated NaCl solution for 120 min, respectively. Na^+-rich PAM/PEG/SA-Na, PAM/PEG/SA/CNTs-Na, and PAM/PEG/SA/S-CNTs-Na hydrogels were obtained (see the Supplementary Information experiment section for details). For convenience, in some illustrations, samples are abbreviated as PAM/PEG (PPM), PAM/PEG/SA(PPS),PAM/PEG/SA/CNTsC(PPSC),PAM/PEG/SA/S-CNTs (PPSC-S), and PAM/PEG/SA-Na (PPS-Na), PAM/PEG/SA/CNTs-Na (PPSC-S-Na), and PAM/PEG/SA/S-CNTs-Na (PPSC-S-Na).

3. Results and discussion

3.1. Morphology of PAM/PEG/SA/S-CNTs-Na hydrogels

In order to study the microstructure of the prepared hydrogel, the morphology of the hydrogel after drying was observed by scanning electron microscope (SEM), as shown in Fig. 2(a)–(f). Compared with PAM/PEG/SA hydrogels (Fig. 2(a)), PAM/PEG/SA/CNTs hydrogels (Fig. 2(b)) have obvious pore structure and more obvious lamellar structure, but their material orientation is disorderly. On the contrary, when CNTs were modified by SDBS, the resulting hydrogels of PAM/PEG/SA/S-CNTs grew toward the lower right, and their structures were arranged in a regular manner (Fig. 2(c)). In addition, by soaking the hydrogel in 10wt% NaCl solution (Fig. 2(d)–(f)), the pore size of PAM/PEG/SA-Na hydrogel increased (Fig. 2(d)), which is due to the excessive Na^+ inhalation, which expands the hydrogel and increases its pore size [25]. In Fig. 2(e) and (f), the PAM/PEG/SA/CNTs-Na and PAM/PEG/SA/S-CNTs-Na hydrogels has an obvious massive structure, and its morphology is like a coral reef. In addition, the element mapping image of PAM/PEG/SA/S-CNTs-Na hydrogel (Fig. 2(g)) shows a uniform distribution of C, N, O, and Na.

The FTIR spectral image of the hydrogel (Fig. 2(h) and (i)) shows that the prepared hydrogel has a C–C stretching band at about 1082 cm^{-1}, and the characteristic peak formed is C–C stretching vibration in PAM. A characteristic peak was observed at around 1648 cm^{-1}, which is due to the stretching vibration of C=O [26]. The tensile vibration of C–H is about 2881 cm^{-1}. In addition, the tensile vibration peak of –OH is found at 3342–3394 cm^{-1} [27]. Among them, compared with PAM/PEG hydrogels, with the addition and modification of different substances, the absorption peaks of C–C and C–H bonds have different degrees of blue shift, and the absorption strength decreases, and the absorption peaks of O–H bonds have different degrees of red shift, and the absorption strength increases. However, the main components of the hydrogel cross-linked with Na^+ did not form new absorption peaks, so no new substances were formed. However, the introduction of Na^+ induced the self-assembly effect of sodium alginate, promoted the densification of the internal structure of the hydrogel, and caused certain changes in its structure, resulting in varying degrees of changes in the intensity of the absorption peaks (Fig. 2(i)).

XRD provides strong evidence for the existence of physical cross-linking in microregions. It can be seen from Fig. 2(j) that with the addition of SA, CNTs, and S-CNTs, the characteristic peaks of PAM/PEG at 36.34° gradually become smooth, and the strength of the characteristic peaks at 20.61° increase. Large characteristic peaks of PAM/PEG at about 22° can be clearly seen, and their peaks were 21.65°, 22.43°, and 22.43°, respectively. The results show that the introduction of SA, CNTs, and S-CNTs has significant effects on the crystallinity of PAM/PEG hydrogels, in which the introduction of SA has the greatest effect on the crystallinity of PAM/PEG hydrogels. Surprisingly, the introduction of Na^+ resulted in many sharp characteristic peaks in PAM/PEG/SA-Na, PAM/PEG/SA/CNTs-Na, and PAM/PEG/SA/S-CNTs-Na hydrogels (Fig. 2(k)), all of which crystallized similar to the XRD of NaCl (PDF #05-0628).

3.2. Characterization of PAM/PEG/SA/S-CNTs-Na hydrogels

In order to further investigate the mechanical properties of hydrogels, the mechanical properties of PAM/PEG, PAM/PEG/SA, PAM/PEG/SA/CNTs, and PAM/PEG/SA/S-CNTs hydrogels were studied, and compression tests were carried out on the samples. As shown in Fig. 3(a)–(d), the compressive stress and ultimate strain of the hydrogels incorporated with SA, CNTs, and SDBS is significantly improved compared with that of PAM/PEG hydrogels. First, the presence of CNTs and S-CNTs causes entanglement and electrostatic attraction within the hydrogel [28–30]. Secondly, the self-assembly of SA induced by the introduction of Na^+ improves the crystallinity of PAM/PEG/SA-Na, PAM/PEG/SA/CNTs-Na, and PAM/PEG/SA/S-CNTs-Na hydrogels and densifies their internal structures [31]. These effects work together to provide a highly malleable support structure for hydrogels.

The PAM/PEG/SA/CNTs hydrogel had the highest compressive stress and ultimate strain and were 18.70 MPa and 48.86%, respectively, which is 5.6% and 21.8% higher than PAM/PEG hydrogel (Fig. 3(a) and (c)). As expected, the stress–strain of the hydrogels soaked in Na^+ solution was improved (Fig. 3(b) and (d)), and the compressive stresses of PAM/PEG/SA/CNT-Na and PAM/PEG/SA/S-CNT-Na hydrogels increased to 19.18 MPa and 19.05 MPa, respectively. Compared with before Na^+ immersion, the increase was 2.57% and 3.03%, respectively. Furthermore, it can be seen from Fig. 3(e)–(i) that PAM/PEG/SA/S-CNTs-Na hydrogels have good resilient deformation and recovery rate.

The electrical conductivity of PAM/PEG/SA and PAM/PEG/SA/S-CNTs hydrogels was characterized by light-emitting diode (LED)-assisted characterization techniques (Fig. 4(a)–(d). The incorporation of SA helps to improve the conductivity of hydrogel, which increases from 0.179 to 0.197 s/m (Fig. 4(e)). As expected, CNTs wound around each other to form a tightly connected conductive network, thereby increasing the conductivity to 0.204 s/m (Fig. 4(e)). Finally, PAM/PEG/SA/CNTs hydrogel were modified with SDBS to enhance their electrical conductivity up to 0.377 s/m (Fig. 4(f)).This is because the porous structure inside the PAM/

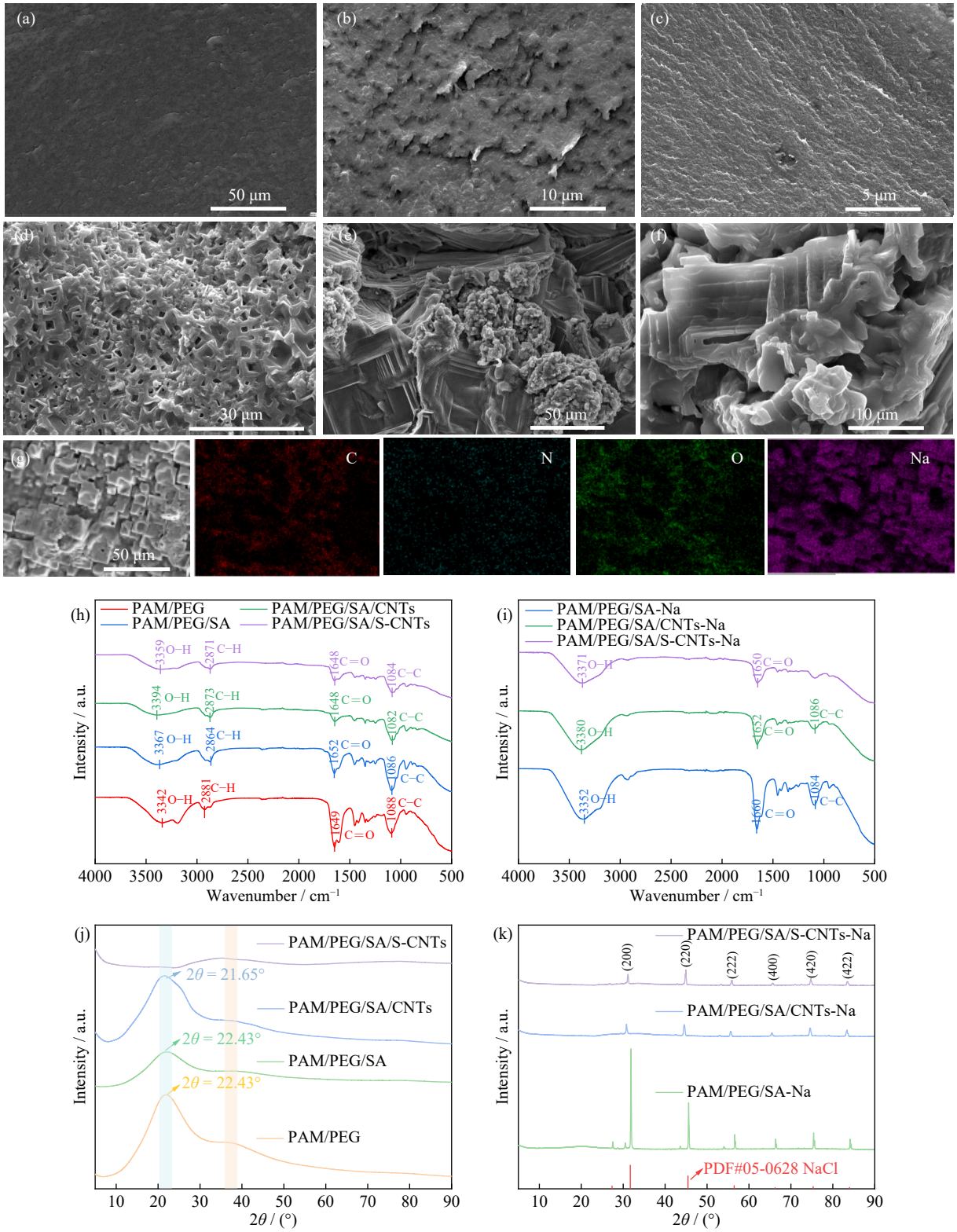

Fig. 2. (a–f) SEM images of underwater gels: (a) PAM/PEG/SA; (b) PAM/PEG/SA/CNTs; (c) PAM/PEG/SA/S-CNTs; (d) PAM/PEG/SA-Na; (e) PAM/PEG/SA/CNTs-Na; (f) PAM/PEG/SA/S-CNTs-Na. (g) Energy dispersive spectrometer (EDS) spectra of PAM/PEG/SA/S-CNTs-Na hydrogels, (h, i) Fourier transform infrared spectroscopy (FTIR) spectrogram of different hydrogels, and (j, k) X-ray diffraction (XRD) pattern of different hydrogels.

PEG/SA/CNTs hydrogel was filled with a large amount of water, and the close packing of S-CNTs in the pore wall would bring about the volume exclusion effect, forming a better conductive path [30]. Surprisingly, with the introduction of Na^+, PAM/PEG/SA-Na, PAM/PEG/SA/CNT-Na, and PAM/PEG/SA/S-CNTs-Na hydrogels allow ions to move freely in their internal networks, moving in a directional manner in response to electric field forces, thus providing high electrical conductivity [32–33], and a brighter LED light is produced (Fig. S1, see the Supplementary Information).

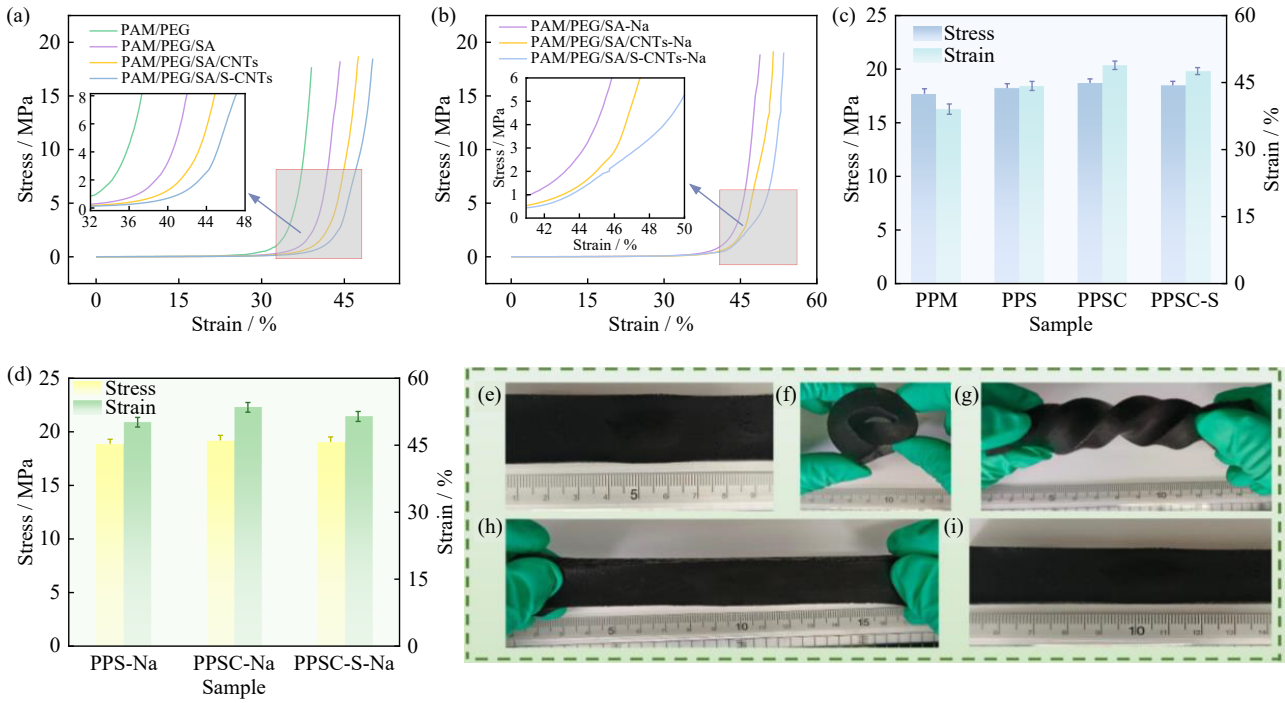

Fig. 3. (a, b) Stress–strain curves of different hydrogels (compression), (c, d) stress and ultimate strain (compression) of different hydrogels. Toughness characterization photos of PAM/PEG/SA/S-CNTs-Na: (e) raw; (f) curved; (g) multi-segment twist; (h) stretch; (i) rehabilitate.

Their conductivities increased to 6.949, 6.988, and 7.794 s/m (Fig. 4(f)), which were 3427.411%, 3325.490%, and 1967.374% higher than that of hydrogels without Na^+ solution, respectively.

Water content and swelling rate of hydrogels were calculated by Eqs. (S1) and (S2), and the results are shown in Fig. 4(g) and (h). The water content and swelling rate of PAM/PEG hydrogels (69.91wt% and 469.24wt%) were higher than those of PAM/PEG/SA, PAM/PEG/SA/CNTs, and PAM/PEG/SA/S-CNTs, which are 61.99wt% and 456.66%, 62.01wt% and 458.84%, 60.58wt% and 423.80%, respectively. The lowest water content was found in the modified PAM/PEG/SA/S-CNTs hydrogels, which is due to the agglomeration of S-CNTs, the decrease of hydrophilicity of S-CNTs, the cross-linking of hydrogels, and the entanglement and collapsing of their pores on the penetration of water molecules [34–35], which leads to the decrease of their water content and solubility, but they were all greater than 60wt% (Fig. 4(g)). Surprisingly, Na^+ migration increased the water content and swelling rate of PAM/PEG/SA-Na, PAM/PEG/SA/CNTs-Na, and PAM/PEG/SA/S-CNTs-Na hydrogels with 66.45wt% and 229.56%, 68.33wt% and 261.59%, 63.70wt% and 113.10%, respectively (Fig. 4(h)). However, the water content of the PAM/PEG/SA/CNTs-Na hydrogel with the highest water content in Na^+ solution-soaked hydrogels (68.33wt%) is also lower than that of PAM/PEG hydrogel (69.91wt%).

Fig. 4(i) shows that although the PAM/PEG/SA/S-CNTs hydrogel has the smallest water content, its apparent density is the largest, and the water content of hydrogel is inversely proportional to its apparent density. Besides, comparing Fig. 4(i) and (j), it can be seen that the apparent densities of hydrogels were reduced to different degrees after under Na^+ solution soak. This is because Na^+ can better fill the void of the material, resulting in larger expansion of the hydrogel and lower density when Na^+ solution is sucked into the solid hydrogel material [35]. Fig. 4(k) and (l) is the swelling curve of each hydrogel. It can be seen that each hydrogel absorbs water rapidly and expands in volume before 6 h of immersion. After 6 h, the swelling efficiency reaches saturation and the swelling curve tends to be flat. The swelling rate was obtained by calculating the mass of each hydrogel after 24 h.

On the basis of studying the conductivity of hydrogel, the electromagnetic shielding performance of hydrogel was further characterized. The EMI SE of hydrogels is shown in Fig. 5(a)–(f), and its change rule is consistent with that of electrical conductivity. The average total EMI SE ($\eta_{SE,T}$) of PAM/PEG hydrogel in the X-band (8.2–12.4Hz) was 15.44 dB (Fig. 5(e)), and the EMI SE of hydrogels mixed with SA, CNTs, and SDBS was improved Fig. 5(a) and (e). Among them, the average $\eta_{SE,T}$ was increased to 16.79, 23.01, and 25.26 dB, respectively, as shown in Fig. 5(e), which basically meets the commercial requirements of 20 dB and achieves moderate electromagnetic interference [36]. As expected, with the introduction of Na^+, the EMI SE of the prepared hydrogels was significantly improved (Fig. 5(b)), with the mean $\eta_{SE,T}$ increasing to 23.80 dB, 28.89 dB, and 32.92 dB (Fig. 5(f)), respectively, 41.75%, 25.55%, and 30.32% higher than that of the hydrogels without Na^+ solution. In order to clarify the electromagnetic shielding mechanism of hydrogel, the reflected EMI SE ($\eta_{SE,R}$), and absorbed EMI SE ($\eta_{SE,A}$) values of hydrogel materials are also given in Fig. 5(c) and (d). As can be seen from Fig. 5(c) and (d), $\eta_{SE,R}$ remained relatively constant, but $\eta_{SE,A}$ gradually increased with the incorporation of

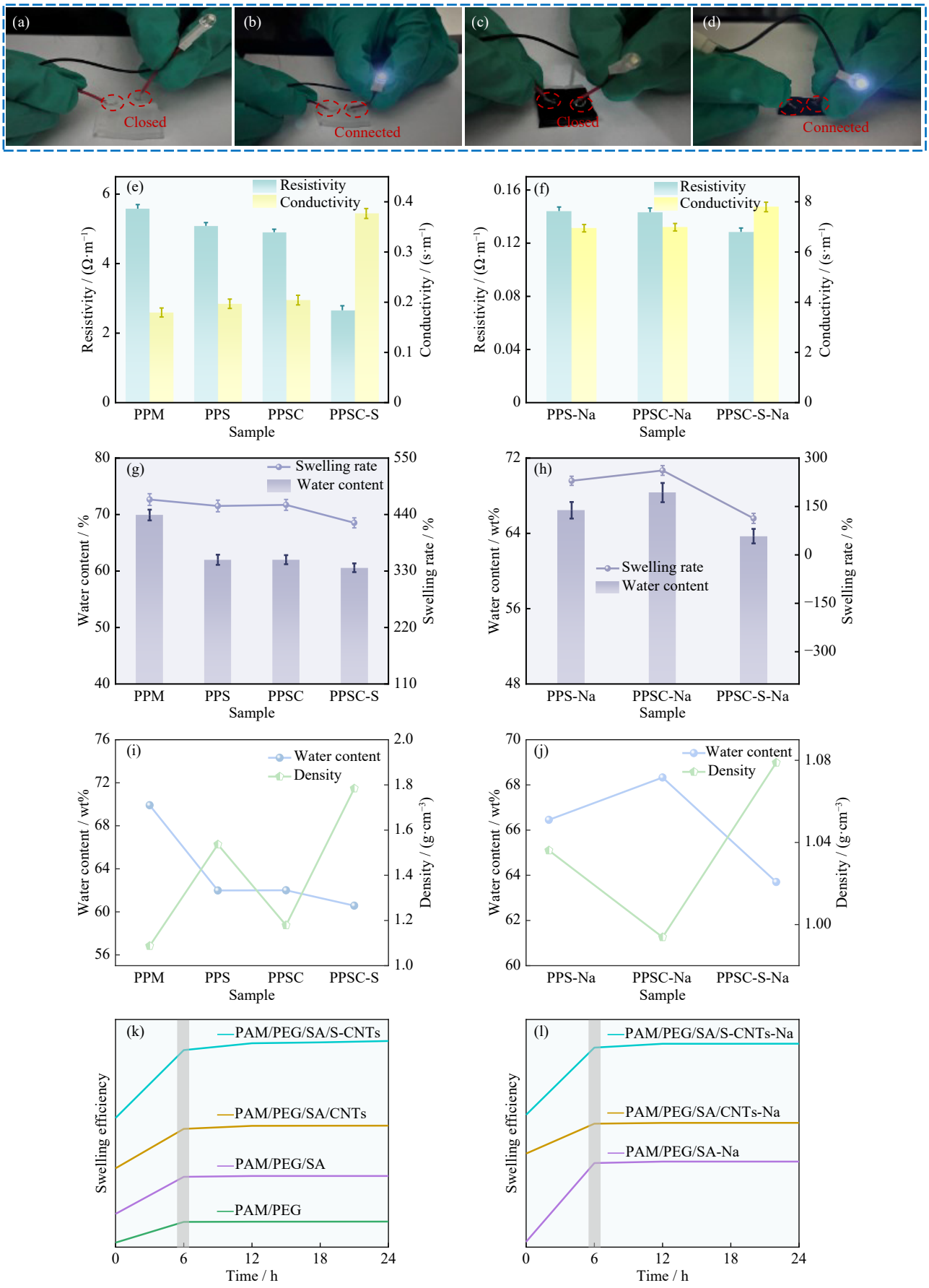

Fig. 4. (a, b) Conductivity photograph of PAM/PEG/SA and (c, d) PAM/PEG/SA/S-CNTs hydrogels; (e, f) conductivity and resistivity of different hydrogels; (g, h) swelling rate and water content of different hydrogels; (i, j) water content and apparent density of different hydrogels; (k, l) swelling curves of different hydrogels.

SA, CNTs, and SDBS. Moreover, with the introduction of Na^+. This trend is also evident in Fig. 5(e) and (f). Fig. 5(g) and (h) shows that the absorption coefficient (A) is always high, while the reflection coefficient (R) is always low and decreasing, indicating that the main EMI mechanism of the prepared hydrogel is absorption rather than reflection (Fig. 5(i)).

In this study, after the introduction of SA molecules, they will dissociate into negatively charged ions in water, which will subsequently bind to Na^+, promoting the self-assembly of SA. With the migration of Na^+, the crystallinity of PAM/PEG/SA-Na, PAM/PEG/SA/CNTs-Na, and PAM/PEG/SA/S-CNTs-Na hydrogels also increased, and the molecules in the crystals were arranged tightly and neatly, which was conducive to ion transfer. Therefore, enhances the characteristics of the conduction path through crosslinking, reduces the resistance of impedance adaptation, so as to achieve effective magnetic field reflection and dissipation, so that electromagnetic shielding has been greatly improved [37–39]. In addition, with the addition of CNTs, an increasingly rich and continuous network provides more electron transport channels. In addition, since the conductivity of SA, CNTs, and S-CNTs hydrogels is inconsistent with that of PAM/PEG hydrogels, polarization loss can also be effectively improved [40–41]. Therefore, total EMI SE and absorbed EMI SE increase significantly due to these dopants enhancing the conductivity and polarization loss of the hydrogel.

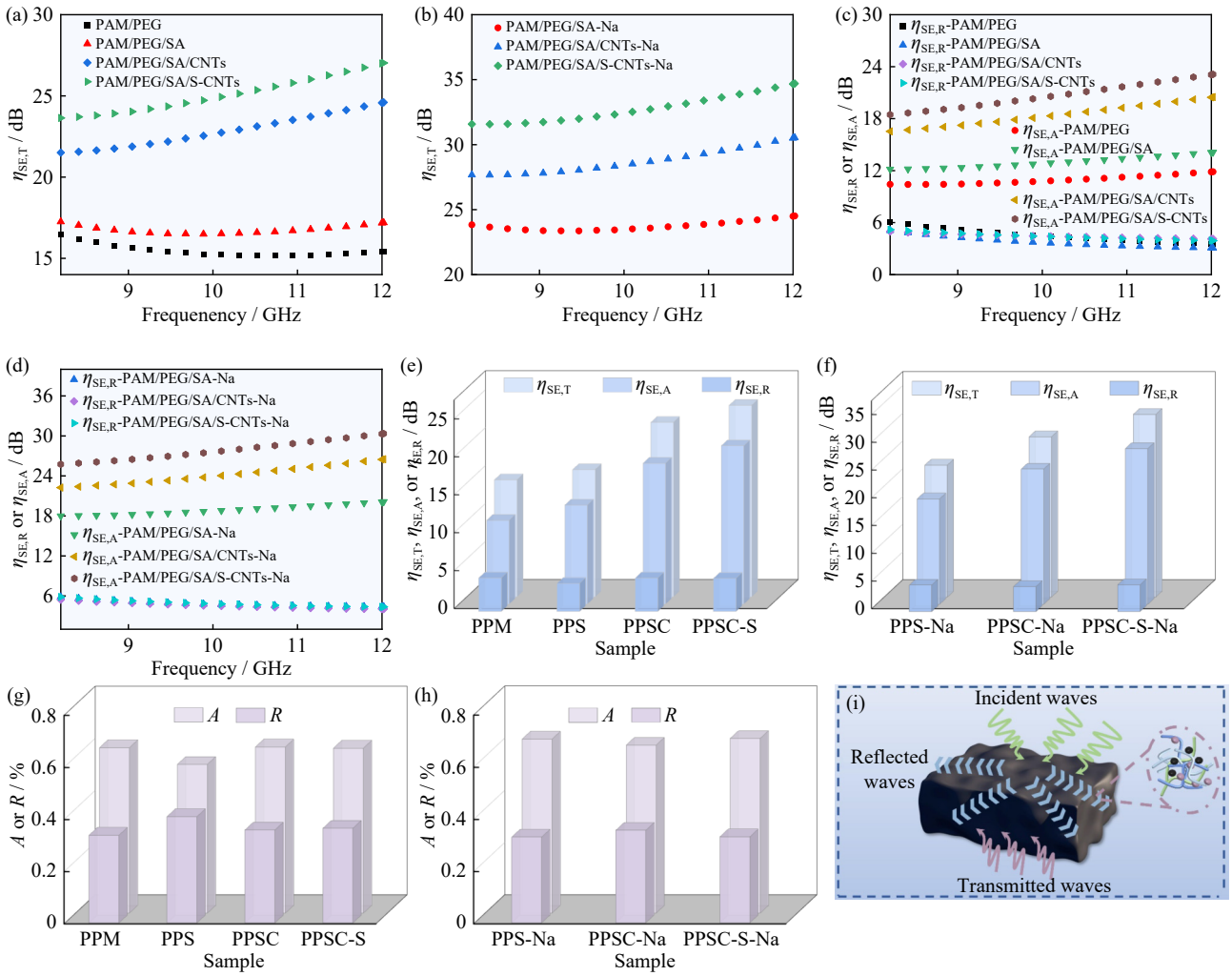

Fig. 5. (a, b) Total EMI SE ($\eta_{SE,T}$) of different hydrogels; (c, d) reflected EMI SE ($\eta_{SE,R}$) and absorbed EMI SE ($\eta_{SE,A}$) of different hydrogels; (e, f) average $\eta_{SE,T}$, $\eta_{SE,R}$, and $\eta_{SE,A}$ of different hydrogels; (g, h) absorption coefficient (A) and the reflection coefficient (R) of different hydrogels; (i) electromagnetic shielding mechanism diagram.

In short, there are a lot of interfaces inside PAM/PEG/SA/S-CNTs hydrogels, and electromagnetic energy loss and dielectric loss will be absorbed and attenuated through the interface structure inside the hydrogels [42]. In addition, with the introduction of Na^+, the formation of ion transfer channels is promoted, thus achieving the ideal electromagnetic shielding efficiency. In summary, PAM/PEG/SA/S-CNTs-Na hydrogel is an electromagnetic shielding material with an EMI SE of up to 32.92 dB, which is an absorption-based electromagnetic shielding material.

4. Conclusion

In this study, PAM/PEG/SA/S-CNTs-Na hydrogels with

well mechanical strength and electromagnetic shielding properties were prepared by a simple one-bath method. Firstly, AM monomer is thermally induced *in situ* polymerization of free radicals to form PAM, and the resulting PAM is blended with PEG to prepare PAM/PEG hydrogels to form rigid support structures. Subsequently, SDBS modified S-CNTs were incorporated into SA and PAM/PEG, and finally Na^+ was used to trigger the self-assembly of SA, which significantly improved the mechanical properties and electrical conductivity of the hydrogel. The compressive strength of PAM/PEG/SA/S-CNTs-Na hydrogel prepared was 19.05 MPa, and the electromagnetic interference efficiency was as high as 32.92 dB when the thickness was only 3 mm and the CNTs content was 16.53wt%. This innovative inorganic nanocomposite hydrogel material is cheap to manufacture, does not pollute the environment, and is easy to biodegrade, which may be a feasible solution to the problem of harmful electromagnetic waves.

Acknowledgements

This work was financially supported by the National Natural Science Foundation of China (No. 52163001), the Guizhou Provincial Science and Technology Program Project Grant, China (Qiankehe Platform Talents-CXTD [2021]005, Qiankehe Platform Talents-GCC [2022]010-1, Qiankehe Fuqi [2023]001, Qiankehe Platform Talents-GCC [2023]035, and Qiankehe Platform Talents-CXTD [2023]003), the Guizhou Minzu University Research Platform Grant, China (No. GZMUGCZX [2021]01), the Central Guided Local Science and Technology Development Funds Project, China (Qiankehe Zhong Yindi [2023]035), the Green Chemistry and Resource Environment Innovation Team of Guizhou Higher Education Institutions, China (Guizhou Education and Technology [2022]No. 13), and the Doctor Startup Fund of Guizhou Minzu University, China (No. GZMUZK [2024]QD77).

Conflict of Interest

The authors declare no conflict of interest.

Supplementary Information

The online version contains supplementary material available at https://doi.org/10.1007/s12613-024-3012-7.

References

[1] J.H. Wen, D. Lan, Y.Q. Wang, *et al*., Absorption properties and mechanism of lightweight and broadband electromagnetic wave-absorbing porous carbon by the swelling treatment, *Int. J. Miner. Metall. Mater.*, 31(2024), No. 7, p. 1701.

[2] X.Q. Yang, H.H. Wang, J. Chen, *et al*., Customization of FeNi alloy nanosheet arrays inserted with biomass-derived carbon templates for boosted electromagnetic wave absorption, *Int. J. Miner. Metall. Mater.*, 31(2024), No. 4, p. 812.

[3] X.B. Xie, H.S. Wang, H. Kimura, C. Ni, W. Du, and G.L. Wu, NiCoZn/C@melamine sponge-derived carbon composites with high-performance electromagnetic wave absorption, *Int. J. Miner. Metall. Mater.*, 31(2024), No. 10, p. 2274.

[4] M.H. Yuan and H.J. Wang, Robust and ultra-flexible PVDF composite film towards electromagnetic interference shielding and active personal thermal management, *Prog. Org. Coat.*, 189(2024), art. No. 108362.

[5] J.M. Yang, H. Wang, Y.L. Zhang, H.X. Zhang, and J.W. Gu, Layered structural PBAT composite foams for efficient electromagnetic interference shielding, *Nano Micro Lett.*, 16(2024), art. No. 31.

[6] Y.L. Zhang, K.P. Ruan, K. Zhou, and J.W. Gu, Controlled distributed $Ti_3C_2T_x$ hollow microspheres on thermally conductive polyimide composite films for excellent electromagnetic interference shielding, *Adv. Mater.*, 35(2023), No. 16, art. No. 2211642.

[7] T.T. Li, X.M. Wang, Y.T. Wang, *et al*., Fe_3O_4 and Ag micro/nano coating for high-efficiency flame retardancy and electromagnetic interference shielding, *Prog. Org. Coat.*, 181(2023), art. No. 107563.

[8] M.K. Li, Y.Y. Sun, D.Y. Feng, K.P. Ruan, X. Liu, and J.W. Gu, Thermally conductive polyvinyl alcohol composite films via introducing hetero-structured MXene@silver fillers, *Nano Res.*, 16(2023), No. 5, p. 7820.

[9] W.X. Chen and H.L. Xing, Construction of enhanced multi-polarization and high performance electromagnetic wave absorption by self-growing $ZnFe_2O_4$ on Cu_9S_5, *Int. J. Miner. Metall. Mater.*, 31(2024), No. 8, p. 1922.

[10] P. Kaur, S. Bindra Narang, and S. Bahel, Complex permittivity, complex permeability and reflection loss of Co–Zr substituted La–Sr hexaferrites in 18–40 GHz frequency range, *J. Magn. Magn. Mater.*, 502(2020), art. No. 166456.

[11] F.M. Oliveira and R. Gusmão, Recent advances in the electromagnetic interference shielding of 2D materials beyond graphene, *ACS Appl. Electron. Mater.*, 2(2020), No. 10, p. 3048.

[12] P. Song, B. Liu, C.B. Liang, *et al*., Lightweight, flexible cellulose-derived carbon aerogel@reduced graphene oxide/PDMS composites with outstanding EMI shielding performances and excellent thermal conductivities, *Nano Micro Lett.*, 13(2021), No. 1, art. No. 91.

[13] Q. Su, H.Q. Wang, Y.F. He, D.D. Liu, X.X. Huang, and B. Zhong, Preparation of CIP@TiO_2 composite with broadband electromagnetic wave absorption properties, *Int. J. Miner. Metall. Mater.*, 31(2024), No. 1, p. 197.

[14] Y.F. Yang, M.R. Han, W. Liu, N. Wu, and J.R. Liu, Hydrogel-based composites beyond the porous architectures for electromagnetic interference shielding, *Nano Res.*, 15(2022), No. 10, p. 9614.

[15] T.Y. Zhu, W.J. Jiang, S. Wu, *et al*., Multifunctional MXene/PEDOT:PSS-based phase change organohydrogels for electromagnetic interference shielding and medium-low temperature infrared stealth, *ACS Appl. Mater. Interfaces*, 16(2024), No. 12, p. 15372.

[16] T. Hu, G.P. Wu, H.T. Bu, *et al*., An injectable, adhesive, and self-healable composite hydrogel wound dressing with excellent antibacterial activity, *Chem. Eng. J.*, 450(2022), art. No. 138201.

[17] D.K. Li, W. Zhan, W. Zuo, *et al*., Elastic, tough and switchable swelling hydrogels with high entanglements and low crosslinks for water remediation, *Chem. Eng. J.*, 450(2022), art. No. 138417.

[18] W.X. Yang, B.W. Shao, T.Y. Liu, *et al*., Robust and mechanically and electrically self-healing hydrogel for efficient electromagnetic interference shielding, *ACS Appl. Mater. Interfaces*, 10(2018), No. 9, p. 8245.

[19] S.Q. Lu, B. Ouyang, S.M. Han, *et al*., Flexible polypyrrole nan-

otube–polyethylene glycol–polyvinyl alcohol hydrogels for enhanced electromagnetic shielding, *ACS Appl. Nano Mater.*, 5(2022), No. 8, p. 11407.
[20] T. Zhou, X. Zhan, K.L. Diao, *et al.*, RGO loaded Fe_3O_4 strategy to construct high toughness PAM hydrogel for electromagnetic shielding, *Prog. Org. Coat.*, 196(2024), art. No. 108750.
[21] H.R. Zhang, Z.G. Heng, J. Zhou, *et al.*, *In-situ* co-continuous conductive network induced by carbon nanotubes in epoxy composites with enhanced electromagnetic interference shielding performance, *Chem. Eng. J.*, 398(2020), art. No. 125559.
[22] G. Zhu, L. Giraldo Isaza, B. Huang, and A. Dufresne, Multifunctional nanocellulose/carbon nanotube composite aerogels for high-efficiency electromagnetic interference shielding, *ACS Sustainable Chem. Eng.*, 10(2022), No. 7, p. 2397.
[23] W. Li, L.Q. Tao, M.C. Kang, *et al.*, Tunable mechanical, self-healing hydrogels driven by sodium alginate and modified carbon nanotubes for health monitoring, *Carbohydr. Polym.*, 295(2022), art. No. 119854.
[24] C.Z. Qi, X.Y. Wu, J. Liu, X.J. Luo, H.B. Zhang, and Z.Z. Yu, Highly conductive calcium ion-reinforced MXene/sodium alginate aerogel meshes by direct ink writing for electromagnetic interference shielding and Joule heating, *J. Mater. Sci. Technol.*, 135(2023), p. 213.
[25] X.H. Zhang, H.M. Geng, X.H. Zhang, Y.Q. Liu, J.C. Hao, and J.W. Cui, Modulation of double-network hydrogels via seeding calcium carbonate microparticles for the engineering of ultrasensitive wearable sensors, *J. Mater. Chem. A*, 11(2023), No. 6, p. 2996.
[26] C.X. Li, X.X. Ni, Y. Lei, S.Y. Li, L. Jin, and B. You, Plasmolysis-inspired yolk–shell hydrogel-core@void@MXene-shell microspheres with strong electromagnetic interference shielding performance, *J. Mater. Chem. A*, 9(2021), No. 47, p. 26839.
[27] Y.H. Xu, X. Zhan, J.Y. Du, Z.L. Wu, and D.H. Zhang, Fluorescent hydrogel with high toughness response based on lanthanide metals: Material Adhesion, multicolor Modulation, information encryption, *Chem. Eng. J.*, 489(2024), art. No. 151303.
[28] W.J. Yang, R. Zhang, X. Guo, *et al.*, Supramolecular polyelectrolyte hydrogel based on conjoined double-networks for multifunctional applications, *J. Mater. Chem. A*, 10(2022), No. 44, p. 23649.
[29] Y.H. Xu, M. Pei, J.Y. Du, *et al.*, A tough, anticorrosive hydrogel consisting of bio-friendly resources for conductive and electromagnetic shielding materials, *New J. Chem.*, 47(2023), No. 29, p. 13721.
[30] Q.F. Guan, Z.M. Han, K.P. Yang, *et al.*, Sustainable double-network structural materials for electromagnetic shielding, *Nano Lett.*, 21(2021), No. 6, p. 2532.
[31] X.C. Jiang, N.P. Xiang, H.X. Zhang, Y.J. Sun, Z. Lin, and L.X. Hou, Preparation and characterization of poly(vinyl alcohol)/sodium alginate hydrogel with high toughness and electric conductivity, *Carbohydr. Polym.*, 186(2018), p. 377.
[32] S. Abolpour Moshizi, H. Moradi, S.Y. Wu, Z.J. Han, A. Razmjou, and M. Asadnia, Biomimetic ultraflexible piezoresistive flow sensor based on graphene nanosheets and PVA hydrogel, *Adv. Mater. Technol.*, 7(2022), No. 1, art. No. 2100783.
[33] M. Qin, W.F. Yuan, X.M. Zhang, *et al.*, Preparation of PAA/PAM/MXene/TA hydrogel with antioxidant, healable ability as strain sensor, *Colloids Surf. B*, 214(2022), art. No. 112482.
[34] O.D. Hu, G.Q. Chen, J.F. Gu, *et al.*, A facile preparation method for anti-freezing, tough, transparent, conductive and thermoplastic poly(vinyl alcohol)/sodium alginate/glycerol organohydrogel electrolyte, *Int. J. Biol. Macromol.*, 164(2020), p. 2512.
[35] J.Y. Tian, Z. Sun, C. Shi, and Z.H. Huang, Rapid fabrication of tough sodium alginate/MXene/poly(vinyl alcohol) dual-network hydrogel electrolytes for flexible all-solid-state supercapacitors, *Int. J. Biol. Macromol.*, 248(2023), art. No. 125937.
[36] Z. Zeng, C. Wang, G. Siqueira, *et al.*, Nanocellulose-MXene biomimetic aerogels with orientation-tunable electromagnetic interference shielding performance, *Adv. Sci.*, 7(2020), No. 15, art. No. 2000979.
[37] J. Liu, M.Y. Yu, Z.Z. Yu, and V. Nicolosi, Design and advanced manufacturing of electromagnetic interference shielding materials, *Mater. Today*, 66(2023), p. 245.
[38] X.T. Liu, K. Pang, H.S. Qin, *et al.*, Hyperbolic graphene framework with optimum efficiency for conductive composites, *ACS Nano*, 16(2022), No. 9, p. 14703.
[39] Q.M. Zhang, Q. Wang, J. Cui, *et al.*, Structural design and preparation of $Ti_3C_2T_x$ MXene/polymer composites for absorption-dominated electromagnetic interference shielding, *Nanoscale Adv.*, 5(2023), No. 14, p. 3549.
[40] R. Yin, C. Zhang, J. Shao, *et al.*, Integration of flexible, recyclable, and transient gelatin hydrogels toward multifunctional electronics, *J. Mater. Sci. Technol.*, 145(2023), p. 83.
[41] Y.Y. Zhu, J. Liu, T. Guo, J.J. Wang, X.Z. Tang, and V. Nicolosi, Multifunctional $Ti_3C_2T_x$ MXene composite hydrogels with strain sensitivity toward absorption-dominated electromagnetic-interference shielding, *ACS Nano*, 15(2021), No. 1, p. 1465.
[42] C.C. Yu, S.P. Zhu, C.T. Xing, *et al.*, Fe nanoparticles and CNTs co-decorated porous carbon/graphene foam composite for excellent electromagnetic interference shielding performance, *J. Alloys Compd.*, 820(2020), art. No. 153108.